AIP Journal of Applied Physics

Dynamic magnetic hysteresis and nonlinear susceptibility of antiferromagnetic nanoparticles

Yuri P. Kalmykov, Bachir Ouari, and Serguey V. Titov

Citation: Journal of Applied Physics **120**, 053901 (2016); doi: 10.1063/1.4959816
View online: http://dx.doi.org/10.1063/1.4959816
View Table of Contents: http://scitation.aip.org/content/aip/journal/jap/120/5?ver=pdfcov
Published by the AIP Publishing

JOURNAL OF APPLIED PHYSICS **120**, 053901 (2016)

Dynamic magnetic hysteresis and nonlinear susceptibility of antiferromagnetic nanoparticles

Yuri P. Kalmykov,[1] Bachir Ouari,[2] and Serguey V. Titov[3]
[1]*Laboratoire de Mathématiques et Physique (LAMPS, EA 4217), Université de Perpignan Via Domitia, F-66860, Perpignan, France*
[2]*Physics Department, University of Tlemcen, BP 119 Chetouane, Tlemcen, Algeria*
[3]*Kotelnikov's Institute of Radio Engineering and Electronics of the Russian Academy of Sciences, Vvedenskii Square 1, Fryazino, Moscow Region, 141190, Russian Federation*

(Received 11 February 2016; accepted 14 July 2016; published online 1 August 2016)

The nonlinear ac stationary response of antiferromagnetic nanoparticles subjected to both external ac and dc fields of arbitrary strength and orientation is investigated using Brown's continuous diffusion model. The nonlinear complex susceptibility and dynamic magnetic hysteresis (DMH) loops of an individual antiferromagnetic nanoparticle are evaluated and compared with the linear regime for extensive ranges of the anisotropy, the ac and dc magnetic fields, damping, and the specific antiferromagnetic parameter. It is shown that the shape and area of the DMH loops of antiferromagnetic particles are substantially altered by applying a dc field that permits tuning of the specific magnetic power loss in the nanoparticles. *Published by AIP Publishing.*
[http://dx.doi.org/10.1063/1.4959816]

I. INTRODUCTION

The physical properties of ferromagnets and antiferromagnets are drastically modified when their dimensions are reduced to the nanometric scale. This fact has prompted both the fabrication of and various studies of the behavior of ferromagnetic and antiferromagnetic nanoparticles with the aim of seeking new properties and applications, especially in data storage[1,2] and medicine.[3–6] Ferromagnetic nanoparticles are characterized by instability of the magnetization due to thermal agitation causing spontaneous change of particle orientation from one metastable state to another resulting in the phenomenon of superparamagnetism.[7,8] Furthermore, due to the large magnetic dipole moment of ferromagnetic nanoparticles ($\sim 10^4$–$10^6 \mu_B$), the Zeeman energy is large even in relatively weak external magnetic fields causing nonlinear effects in the dynamic susceptibility, stochastic resonance, dynamic magnetic hysteresis (DMH), etc. In the case of *antiferromagnetic* nanoparticles, their magnetization dynamics may differ in many respects from those of ferromagnetic ones because of the intrinsic properties of antiferromagnetic materials. Moreover, the magnetic behavior of antiferromagnetic nanoparticles can be quite different from that observed in the bulk, e.g., enhanced magnetic moment and coercivity, exchange bias, increase in magnetic moment with temperature, decrease in the susceptibility with temperature below the ordering (Néel) temperature T_N, and its enhancement compared to that of the bulk.[9] Moreover, due to thermal agitation, antiferromagnetic nanoparticles should become superparamagnetic at finite temperatures just as ferromagnetic nanoparticles (the so-called superantiferromagnetism[10]).

The initial theory of the thermal fluctuations in magnetic nanoparticles due to Néel[7] was further developed by Brown[11,12] and is consequently known as the Néel-Brown model. His treatment utilizes the classical theory of the Brownian motion in conjunction with the Landau-Lifshitz-Gilbert equation[13,14] augmented by random fields regarded as the magnetic Langevin equation governing the thermoactivated transitions of the magnetic moment in a nanoparticle in the coherent rotation approximation. This model may also be adapted to antiferromagnetic nanoparticles. An ideal antiferromagnet can be divided into two sublattices, with equal and opposite magnetic moments. If the numbers N_1 and N_2 of ions in these sublattices are equal, we say, the sample is "compensated." In fine antiferromagnetic particles, total magnetic compensation of the sublattices is impossible for a number of reasons (unequal numbers of spins in crystal planes, spin frustration near the surface, lattice defects, etc.) so that $N_1 \neq N_2$ resulting in the effective spontaneous magnetization in such particles. If we will assume the ionic magnetic moments m remain the same and $N_1 > N_2$, so the total moments of the sublattices $\mathbf{m}_1 = N_1 m\mathbf{u}$ and $\mathbf{m}_2 = -N_2 m\mathbf{u}$ are not equal. Here, $\mathbf{u}$ is the antiferromagnetic vector, which specifies the decompensation magnetic moment $\boldsymbol{\mu} = \mathbf{m}_1 + \mathbf{m}_2 = \mathbf{u}\mu$, where $\mu = m(N_1 - N_2)$. In an antiferromagnetic nanoparticle, an external dc magnetic field $\mathbf{H}_0$ directed along $\mathbf{u}$ will not tend to rotate the moments $\mathbf{m}_1$ and $\mathbf{m}_2$, but a field normal to $\mathbf{u}$ will. Furthermore, an antiferromagnetic nanoparticle possesses a considerable transverse magnetic susceptibility χ_A characterizing the induced magnetic moment of the particle which can be written as $v\chi_A[\mathbf{H}_0 - \mathbf{u}(\mathbf{u}\cdot\mathbf{H}_0)]/2$. Thus, the magnetic moments of two sublattices of the particle with allowance for decompensation can be presented as[9]

$$\mathbf{m}_{1,2} = \left[\pm vM_S + \frac{\mu}{2} - \frac{v\chi_A}{2}(\mathbf{H}_0\cdot\mathbf{u})\right]\mathbf{u}, \tag{1}$$

where $M_S = m(N_1 + N_2)/(2v)$ is the bulk sublattice magnetization and v is the particle volume. Due to a specific superantiferromagnetic effect, χ_A exceeds that of a bulk crystal by a factor of 2 or 3 and attains a typical value of order 10^{-4}

(Refs. 9 and 10), while the magnitude of the magnetic moment $\boldsymbol{\mu}$ can be estimated as $\mu \sim \mu_B (N_1 - N_2)(N_1 + N_2)^{1/2}$,[10] where μ_B is the Bohr magneton, so that for a particle with a diameter $\sim$ 10nm and $N \sim 10^5$–10^6, μ may vary from a few μ_B to few hundred μ_B[15–20] (that is of the same order of magnitude as the magnetization of weak ferromagnets). At temperatures below T_N, as long as the external magnetic fields are much weaker than the exchange field, one may assume[9] that the decompensation magnetic moment is constant in magnitude so that the unit vector $\mathbf{u}$ can only rotate but cannot change its length. Thus, just as in nanoscale ferromagnets, the magnetization dynamics of antiferromagnetic nanoparticles in the presence of thermal agitation can be described using Brown's diffusion model of a magnetic moment (classical spin) via a Fokker-Planck equation for the distribution function $W(\mathbf{u},t)$ of magnetic moment orientations on a unit sphere, viz.,[11,12]

$$\frac{\partial W}{\partial t} = \frac{1}{2\tau_N}\left\{\nabla^2 W + \beta(\nabla \cdot W \nabla V) + \frac{\beta}{\alpha}(\mathbf{u} \cdot [\nabla V \times \nabla W])\right\}, \tag{2}$$

where V is the free-energy of the particle comprising the magnetic anisotropy and Zeeman energy densities, $\tau_N = \tau_0(\alpha + \alpha^{-1})$ is the characteristic free diffusion time, $\tau_0 = \beta\mu_0\mu/(2\gamma)$, $\mu_0 = 4\pi \cdot 10^{-7}\mathrm{JA}^{-2}\mathrm{m}^{-1}$ is the permeability of free space in SI units, $\beta = 1/(kT)$, k is the Boltzmann's constant, T is the absolute temperature, γ is gyromagnetic ratio, and α is the damping parameter. In spherical polar coordinates basis $(\mathbf{e}_r, \mathbf{e}_\vartheta, \mathbf{e}_\varphi)$,[21] $\nabla = \partial/\partial\mathbf{u} = \mathbf{e}_\vartheta \partial_\vartheta + \mathbf{e}_\varphi \csc\vartheta\, \partial_\varphi$ is the gradient operator on the unit sphere, where ϑ and φ are the polar and azimuthal angles, respectively, and $\mathbf{u} = \mathbf{e}_r = (\sin\vartheta\cos\varphi, \sin\vartheta\sin\varphi, \cos\vartheta)$. Without the third (gyromagnetic) term in the right hand side of Eq. (2), the Fokker–Planck equation has the same mathematical form as the diffusion equation for the *noninertial* rotational Brownian motion of a particle in a mean field potential.[9,22] In the simplest case of a uniaxial antiferromagnetic particle, if the easy axis of the nanoparticle coincides with the Z-axis of the laboratory coordinate system, its free energy $V(\vartheta, \varphi, t)$ in superimposed magnetic dc and ac fields $\mathbf{H}(t) = \mathbf{H}_0 + \mathbf{H}_1 \cos\omega t$ is given by[9,10]

$$V(\vartheta, \varphi, t) = vK\sin^2\vartheta - \mu_0\mu H(t)\cos\Theta - \frac{1}{2}v\mu_0\chi_A H^2(t)\sin^2\Theta. \tag{3}$$

Here, $H(t) = H_0 + H_1\cos\omega t$ since the vectors $\mathbf{H}_0$ and $\mathbf{H}_1$ are assumed parallel, Θ is the angle between the unit vectors $\mathbf{u}$ and $\mathbf{h} = \mathbf{H}_0/H_0$ so that

$$\cos\Theta = (\mathbf{u} \cdot \mathbf{h}) = \gamma_1 \sin\vartheta\cos\varphi + \gamma_2\sin\vartheta\sin\varphi + \gamma_3\cos\vartheta,$$

$\gamma_1, \gamma_2, \gamma_3$ are the direction cosines of $\mathbf{H}_0$, and K is the anisotropy constant with an archetypal order of a few 10^4 J/m^3 for ferritin.[16] For $\chi_A = 0$, Eq. (3) yields the free energy for uniaxial ferromagnetic nanoparticles with the anisotropy and Zeeman terms. The last term in the right-hand side of Eq. (3) is a contribution due to the induced moment non-existent for ferromagnetic nanoparticles. This term affects the dynamics of the magnetic moment in the presence of an ac driving field and determines main features of the nonlinear response of nanoscale antiferromagnets. Thus, even moderate external magnetic fields can produce nonlinear effects in the particle magnetization dynamics that may differ from those observed in ferromagnetic nanoparticles.

Using Brown's continuous diffusion model, Raikher and Stepanov[9] have evaluated characteristic relaxation times and the linear dynamic susceptibility of a suspension of antiferromagnetic nanoparticles in the particular case of dc and ac magnetic fields parallel to the easy axis of the particle. Their results were extended in Ref. 23 for the general case when a dc magnetic field is applied at an arbitrary angle to the easy axis. Moreover, the magnetization reversal time τ of antiferromagnetic nanoparticles has been evaluated in Ref. 24 via the Kramers escape rate theory adapted to magnetic nanoparticles;[22,25] the analytic equations for τ so obtained agree favorably with the numerical solution of the Fokker-Planck's equation (2).[23,24] The primary goal of this paper is to give a detailed investigation of the magnetization, nonlinear dynamic magnetic susceptibility, and dynamic magnetic hysteresis (DMH) of antiferromagnetic nanoparticles and to demonstrate that in superimposed dc and ac fields these magnetic characteristics change substantially leading to interesting nonlinear effects. We remark that the theoretical treatment of nonlinear response phenomena inherently poses a complicated mathematical problem because no *unique* response function governing the transient and ac stationary responses, unlike in linear response, exists. However, these difficulties may be overcome by extending the method developed in Refs. 26–32 to the dynamic nonlinear stationary response of ferromagnetic nanoparticles driven by an ac magnetic field. The essential feature of this method is that it allows one to evaluate both the linear and nonlinear ac stationary responses in a wide range of damping and at all frequencies of interest from the very low frequencies up to the very high (GHz) frequencies. If the field $\mathbf{H}_0$ is applied at an arbitrary angle to the easy axis of the particle, a strong intrinsic dependence of magnetic characteristics (such as the reversal time, complex magnetic susceptibility, etc.) on the damping α arising from coupling of the longitudinal and transverse modes of the magnetization exists. As shown by García-Palacios and Svedlindh,[26] the nonlinear dynamical response of nanomagnets in the underdamped regime, $\alpha < 1$, is very sensitive to the damping due to the coupling induced by the driving field between the precession of the magnetic moment and its thermoactivated reversal. The large damping dependence of the nonlinear response can be used to determine the damping coefficient α.[26]

II. BASIC EQUATIONS

For convenience, we introduce the following dimensionless variables: $\sigma = v\beta K$, $\xi_0 = \beta\mu_0\mu H_0$, and $\xi = \beta\mu_0\mu H_1$ are, respectively, the anisotropy, dc, and ac applied field parameters, and $\zeta = v\chi_A/(\beta\mu_0\mu^2)$ is the "antiferromagnetic" parameter. We remark that due to the decompensation origin of the magnetic moment, the field parameters ξ_0 and ξ for

antiferromagnetic nanoparticles are about two orders of magnitude smaller than those for ferromagnetic nanoparticles of the same size $\sim$10 nm.[9] Nonlinear effects (saturation, etc.) in the ac stationary response of antiferromagnetic nanoparticles become pronounced at $\xi > 1$; however, their main features can be studied at $\xi \ll 1$. On seeking the solution of the Fokker-Planck equation (2), where the free energy potential defined by Eq. (3), as a series of spherical harmonics $Y_{lm}(\vartheta, \varphi)$, viz.,

$$W(\vartheta, \varphi, t) = \sum_{l=0}^{\infty} \sum_{m=-l}^{l} c_{lm}(t) Y^*_{lm}(\vartheta, \varphi), \tag{4}$$

the task of calculating the nonlinear ac stationary response of an antiferromagnetic nanoparticle to an external driving field can be reduced[22] to the solution of an infinite hierarchy of 25-term differential-recurrence relation for the statistical moments (the expectation values of the spherical harmonics) $c_{lm}(t)$

$$\begin{aligned}\tau_{\mathrm{N}} \frac{d}{dt} c_{nm}(t) = {} & v^{--}_{nm} c_{n-2m-2}(t) + v^{-}_{nm} c_{n-2m-1}(t) + v_{nm} c_{n-2m}(t) + v^{+}_{nm} c_{n-2m+1}(t) + v^{++}_{nm} c_{n-2m+2}(t) \\ & + w^{--}_{nm} c_{n-1m-2}(t) + w^{-}_{nm}(t) c_{n-1m-1}(t) + w_{nm}(t) c_{n-1m}(t) + w^{+}_{nm}(t) c_{n-1m+1}(t) + w^{++}_{nm} c_{n-1m+2}(t) \\ & + x^{--}_{nm} c_{nm-2}(t) + x^{-}_{nm}(t) c_{nm-1}(t) + x_{nm}(t) c_{nm}(t) + x^{+}_{nm}(t) c_{nm+1}(t) + x^{++}_{nm} c_{nm+2}(t) \\ & + y^{--}_{nm} c_{n+1m-2} + y^{-}_{nm}(t) c_{n+1m-1}(t) + y_{nm}(t) c_{n+1m}(t) + y^{+}_{nm}(t) c_{n+1m+1}(t) + y^{++}_{nm} c_{n+1m+2}(t) \\ & + z^{--}_{nm} c_{n+2m-2}(t) + z^{-}_{nm} c_{n+2m-1}(t) + z_{nm} c_{n+2m}(t) + z^{+}_{nm} c_{n+2m+1}(t) + z^{++}_{nm} c_{n+2m+2}(t).\end{aligned} \tag{5}$$

Here, the asterisks designate the complex conjugate, and the spherical harmonics $Y_{lm}(\vartheta, \varphi)$ are defined as[21]

$$Y_{lm}(\vartheta, \varphi) = (-1)^m \sqrt{\frac{(2l+1)(l-m)!}{4\pi(l+m)!}} e^{im\varphi} P^m_l(\cos\vartheta),$$

$P^m_l(x)$ are the associated Legendre functions[21]

$$c_{lm}(t) = \langle Y_{lm} \rangle(t) = \int_0^{2\pi} \int_0^{\pi} Y_{lm}(\vartheta, \varphi) W(\vartheta, \varphi, t) \sin\vartheta d\vartheta d\varphi, \tag{6}$$

and the time-dependent coefficients $v_{nm}(t)$, $w_{nm}(t)$, $x_{nm}(t)$, etc., are given in the Appendix. Since the ac stationary response is independent of the initial conditions, we need only the steady state solution of Eq. (5) so that $c_{lm}(t)$ can be expanded in a Fourier series as

$$c_{lm}(t) = \sum_{k=-\infty}^{\infty} c^k_{lm}(\omega) e^{ik\omega t}. \tag{7}$$

The Fourier coefficients $c^k_{lm}(\omega)$ can be evaluated using matrix continued fractions (see the Appendix). Consequently, the average magnetic moment of the particle in the direction of the ac driving field

$$\mu_H(t) = \mu[\langle \cos\Theta \rangle(t) + \zeta(\xi_0 + \xi \cos\omega t) \langle \sin^2\Theta \rangle(t)], \tag{8}$$

which is expressed via the statistical moments $\langle Y_{lm} \rangle(t)$ (see Eqs. (A5) and (A6) in the Appendix), can also be presented as a Fourier series

$$\mu_H(t) = \mu \sum_{k=-\infty}^{\infty} m^k_1(\omega) e^{ik\omega t}, \tag{9}$$

where $m^k_1(\omega)$ is the amplitude of the kth harmonic in the nonlinear response given by Eq. (A4) in the Appendix

In order to illustrate the nonlinear effects induced by the ac field, we focus on the *time-independent* or dc component of the magnetization M_ξ defined by the mean value

$$M_\xi = \frac{\omega}{2\pi\mu} \int_0^{2\pi/\omega} \mu_H(t)\, dt = m^0_1(\omega), \tag{10}$$

which we note is entirely real yielding in the limits of *vanishing ac field*, $\xi \to 0$, the static dc magnetization given by

$$\lim_{\xi \to 0} M_\xi = M_0 = \langle \cos\Theta \rangle_0 + \zeta\xi_0 (1 - \langle \cos^2\Theta \rangle_0), \tag{11}$$

where the angular brackets $\langle \quad \rangle_0$ denote equilibrium ensemble averaging defined as

$$\langle \cos^n\Theta \rangle_0 = \frac{1}{Z} \int_0^{2\pi} \int_0^{\pi} \cos^n\Theta\, e^{-E_0(\vartheta,\varphi)} \sin\vartheta d\vartheta d\varphi,$$

$$Z = \int_0^{2\pi} \int_0^{\pi} e^{-E_0(\vartheta,\varphi)} \sin\vartheta d\vartheta d\varphi,$$

is the partition function, and the free energy $E_0(\vartheta, \varphi)$ is given by

$$E_0(\vartheta, \varphi) = \sigma \sin^2\vartheta - \xi_0 \cos\Theta - \frac{\zeta\xi_0^2}{2} \sin^2\Theta. \tag{12}$$

The free energy potential, Eq. (12), has, in general, a bistable structure with two minima separated by a potential barrier with a saddle point.[23] Henceforth, we shall assume without loss of generality that the dc magnetic field vector $\mathbf{H}_0$ lies in the XZ-plane of the laboratory coordinate system making an angle ψ with respect to the easy axis so that the direction cosines of the vector $\mathbf{H}_0$ are $\gamma_1 = \sin\psi$, $\gamma_2 = 0$, and $\gamma_3 = \cos\psi$ yielding

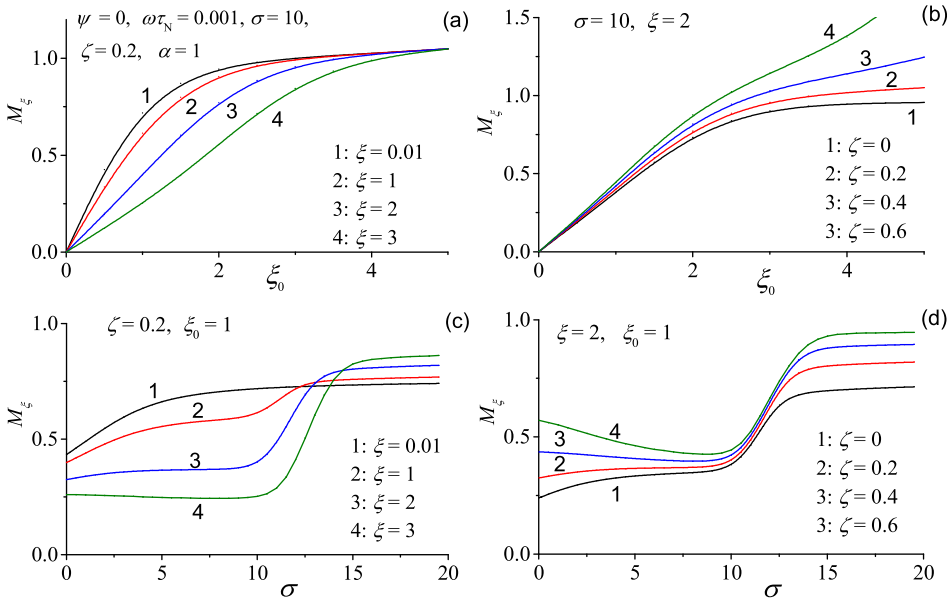

FIG. 1. Dimensionless magnetization M_ξ vs. the dc bias field ((a) and (b)) and anisotropy (inverse temperature) parameters ((c) and (d)) for various ac fields and antiferromagnetic parameters at damping $\alpha = 1$, oblique angle $\psi = 0$, and frequency $\omega\tau_N = 0.001$.

$$\cos\Theta = \cos\psi\cos\vartheta + \sin\psi\sin\vartheta\cos\varphi. \tag{13}$$

Furthermore, we evaluate the spectrum of the fundamental component of the magnetization defined by

$$\chi(\omega) = \frac{6m_1^1(\omega)}{\xi}, \tag{14}$$

which represents the linear and lowest order nonlinear susceptibility. Furthermore, via $m_1^1(\omega)$, we can calculate the dimensionless area of the DMH loop A_n, which is the energy loss per particle and per cycle of the ac field, defined as[33–35]

$$A_n = \frac{1}{4\mu H}\oint \mu_H(t)dH(t) = -\frac{\pi}{2}\mathrm{Im}\left[m_1^1(\omega)\right] \tag{15}$$

(the phenomenon of the DMH in single-domain magnetically *isotropic* nanoparticles was discovered by Ignatchenko and Gekht[36]). The DMH loop represents a parametric plot of the steady-state time-dependent magnetization as a function of the ac field, i.e., $M_H(t) = \mu_H(t)/v$ vs. $H(t) = H\cos\omega t$. All other harmonic components $m_1^k(\omega)$ with $k > 1$ may be investigated in a similar way.

III. RESULTS AND DISCUSSION

In order to illustrate the nonlinear effects in the time-independent but frequency-dependent magnetization, $M_\xi(\omega)$ is plotted in Fig. 1 as a function of the dc field and anisotropy (or the inverse temperature) parameter σ for various ac field magnitudes ξ and antiferromagnetic parameter ζ. The imaginary $\chi''(\omega) = -\mathrm{Im}[\chi(\omega)]$ and the real $\chi'(\omega) = \mathrm{Re}[\chi(\omega)]$ parts of the susceptibility as functions of the anisotropy parameter σ and frequency ω are shown in Figs. 2 and 3, respectively, for various antiferromagnetic parameters ζ both in the linear ($\xi \ll 1$) and nonlinear ($\xi \geq 1$) regimes. (The condition $\xi \to 0$ corresponds to the linear response, where $\mu_H(t)/H_1$ is independent of the ac field strength.) The calculations indicate that a marked dependence of $\chi(\omega)$ on the antiferromagnetic parameter ζ, anisotropy σ, ac field ξ, dc field ξ_0, damping α, and angle ψ exists. For the special case of linear response, $\xi \ll 1$, the results agree with the independent numerical calculations.[24] In strong ac fields, $\xi \geq 1$, pronounced nonlinear effects occur; see Figs. 1–3 illustrating the dependence of the nonlinear response on the ac field parameter ξ. Just as for ferromagnetic nanoparticles,[27–31] three peaks appear in the spectra of the magnetic loss $\chi''(\omega)$ in the neighborhood of frequencies where $\chi'(\omega)$ changes (see Fig. 3). The characteristic frequencies of these peaks, i.e., where $\chi''(\omega)$ reaches local maxima, are τ^{-1}, $\alpha\omega_{\mathrm{pr}}$, and ω_{pr}, where τ is the switching (reversal) time of the magnetic moment between two minima of the free energy separated by a potential barrier with a saddle point, and $\omega_{\mathrm{pr}} = \gamma H_{\mathrm{ef}}$ is the precession frequency of the magnetic moment in the effective magnetic field $\mathbf{H}_{\mathrm{ef}}$. The low-frequency behavior of $\chi'(\omega)$ and $\chi''(\omega)$ is dominated by the barrier-crossing relaxation mode. Here, the reversal time of the magnetization τ can be evaluated from the characteristic frequency $\omega_{\max}$, where

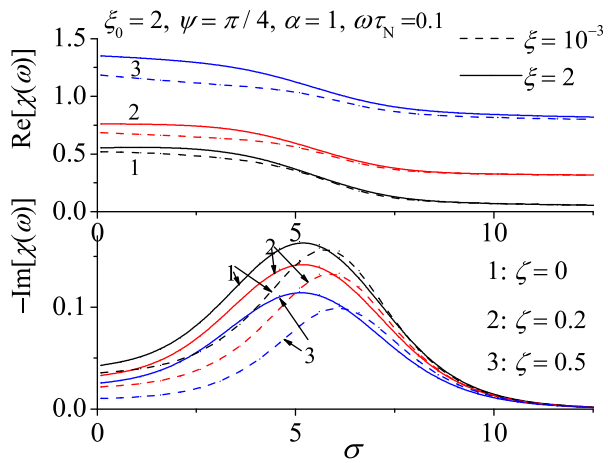

FIG. 2. Real and imaginary parts of the dynamic susceptibility vs. $\sigma \sim T^{-1}$ for various antiferromagnetic parameters ζ at dc field parameter $\xi_0 = 2$, frequency $\omega\tau_N = 0.1$, damping $\alpha = 1$, angle $\psi = \pi/4$, and ac field parameters $\xi = 0.001$ (linear response) and $\xi = 2$ (nonlinear response). Dashed and solid lines: the linear and nonlinear response, respectively.

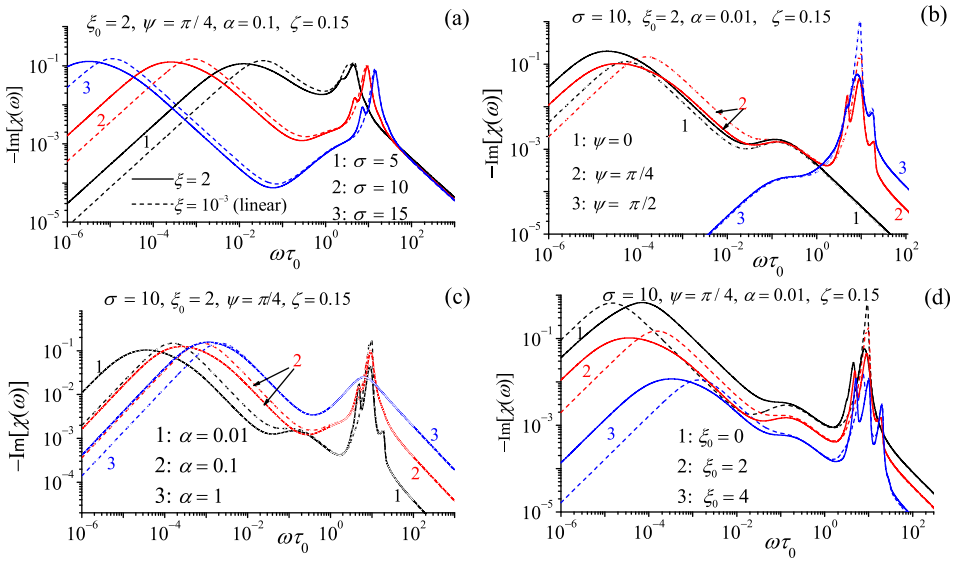

FIG. 3. Imaginary part of the dynamic susceptibility $-\mathrm{Im}[\chi(\omega)]$ vs. the dimensionless frequency $\omega\tau_0$ for (a) various anisotropy parameters σ, (b) angles ψ, (c) damping α, and (d) dc field parameters ξ_0 at the ac field amplitudes $\xi = 0.001$ (linear response: dashed lines) and 2 (nonlinear response: solid lines).

$\chi''(\omega)$ reaches a maximum, and/or the half-width $\Delta\omega$ of the spectrum of $\chi'(\omega)$ as

$$\tau \approx \omega_{\max}^{-1} \approx \Delta\omega^{-1}. \tag{16}$$

In weak ac fields, $\xi \ll 1$, the magnetization reversal time τ can be associated with the inverse of the smallest nonvanishing eigenvalue λ_1 of the Fokker-Planck operator in Eq. (2).[22] In this case, comparison of τ as extracted from the spectra $\chi'(\omega)$ and $\chi''(\omega)$ via Eq. (16) with $\tau = \lambda_1^{-1}$ calculated using the independent method[22] via λ_1 of the Fokker-Planck operator shows that both methods yield identical results. Furthermore, our calculations indicate that when the dc field parameter ξ_0 is increased, the magnitude of the low-frequency peak decreases due to the depletion of the population in the shallowest potential well of the free-energy density $E_0(\vartheta, \varphi)$, Eq. (12); this effect is signified by the virtual disappearance of the low-frequency peak in the magnetic loss spectrum $\chi''(\omega)$ (see Fig. 3(d)). For weak dc bias field, $\xi_0 < 0.3$, the low-frequency peak shifts monotonically to higher frequencies as the ac field amplitude ξ is increased. For strong dc bias field, $\xi_0 > 1$, the low frequency peak shifts to lower frequencies reaching a maximum at $\xi \sim \xi_0$, thereafter decreasing rapidly with increasing ξ. In other words, as the dc field increases, the reversal time of the magnetization *initially increases* and then having attained its maximum at some critical value $\xi \sim \xi_0$ decreases. In addition, a second relaxation peak in $\chi''(\omega)$ and the corresponding dispersion of $\chi'(\omega)$ appearing at higher frequencies $\sim\alpha\omega_{\mathrm{pr}}$ are due to the near degenerate "intrawell" relaxation modes, which are virtually indistinguishable in the frequency spectra. Now for $\xi_0/\sigma < 0.1$, the amplitude of this peak is far weaker than that of the low-frequency one. However, for $\xi_0/\sigma > 0.4$, this peak may come to dominate the spectra because as h_0 increases, the magnitude of the low-frequency peak drastically decreases (see Fig. 3(d)). Figure 3(d) also illustrates the inherent dependence of $\chi(\omega)$ on the damping parameter α arising from the coupling of the longitudinal and transverse relaxation modes.[26] This coupling appears in the dynamical equation of motion of the magnetic moment $\boldsymbol{\mu}(t)$, where its longitudinal component is entangled with the transverse components resulting in the appearance of a third antiferromagnetic resonance (AFMR) peak in the spectrum of $\chi''(\omega)$ due to excitation of transverse modes with characteristic frequencies close to the precession frequency ω_{pr} in the effective magnetic field $\mathbf{H}_{\mathrm{ef}}$ (see Fig. 3). The AFMR peak appears only for low damping ($\alpha \ll 1$) and strongly manifests itself at high frequencies $\omega \sim \omega_{\mathrm{pr}}$ (see Fig. 3(c); a feature which is absent for $\alpha > 1$). As seen in Fig. 3, with increasing ac field ξ, the magnitude of the AFMR peak decreases and the peak half-width broadens showing pronounced nonlinear effects. In addition, a second weak resonance peak owing to parametric resonance of the nonlinear oscillatory (precessional) motion of the magnetic moment $\boldsymbol{\mu}(t)$ appears at frequencies $\sim\omega_{\mathrm{pr}}/2$ (Fig. 3(a)), while for very low damping, $\alpha < 0.01$, resonance peaks with characteristic frequencies $n\omega_{\mathrm{pr}}$, $n = 2, 3, \ldots$ due to the high-frequency resonant modes are discernible in the spectrum (only the peak with $n = 2$ is visible in Figs. 3(b)–3(d)). These peaks virtually disappear, however, for $\psi = 0$. Such nonlinear effects always exist in nonlinear oscillator systems driven by an ac external force.[37]

The DMH loops, i.e., $m(t) = \mu_H(t)/\mu$ vs. $h(t) = H(t)/H = \cos\omega t$, for various antiferromagnetic ζ and inverse temperature $\sigma \propto 1/T$ parameters are presented in Figs. 4 and 5 for a wide range of other model parameters (damping, oblique angle, etc.). At finite temperatures due to thermal motion, the particle magnetic moment is never completely saturated wandering between the "up" and "down" states. Furthermore, the shape of the DMH loops for given values of anisotropy parameter σ, antiferromagnetic parameter ζ, damping α, oblique angle ψ, and dc field ξ_0 depends on the amplitude ξ and frequency ω of the ac field. Figures 4(a) and 4(b) show, respectively, that the shape and area of the DMH loops strongly depend on the anisotropy σ and the dc field parameters ξ_0. In particular, Fig. 4(b) illustrates that the area of the DMH loops decreases with increasing the dc field parameter ξ_0. Also, with decreasing anisotropy parameter σ, i.e., with increasing temperature, the DMH loops become narrow (Fig. 4(a)), which implies that a small amount of energy is used up

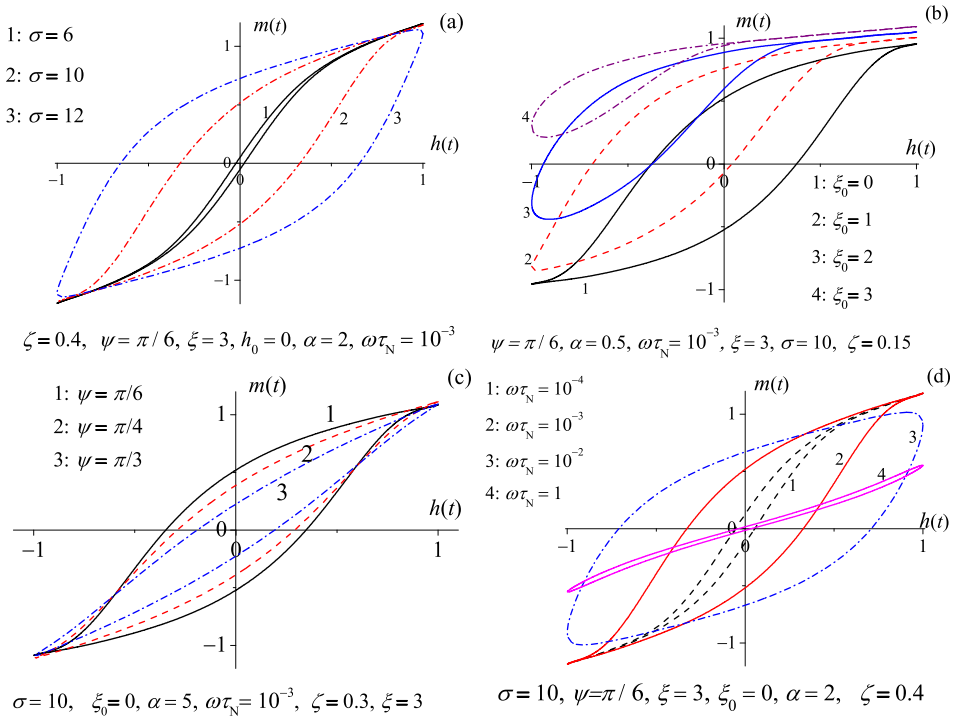

FIG. 4. DMH loops for (a) various anisotropy parameters $\sigma = 6, 10, 12$, (b) dc fields $\xi_0 = 0, 1, 2, 3$, (c) angles $\psi = \pi/6, \pi/4, \pi/3$, and (d) frequency $\omega\tau_N = 10^{-4}, 10^{-3}, 10^{-2}, 1$.

in reversing the magnetization. Figure 4(c) illustrates the dependence of the shape and area of the DMH loops on the oblique angle ψ, while in Fig. 4(d), the DMH loops are presented for very low and intermediate frequencies. At low frequencies, $\omega\tau_N \sim 10^{-4} - 10^{-3}$, the loops are large while at intermediate frequencies, $\omega\tau_N \sim 1$, the shape of loops becomes elliptic with small area. At low frequencies, where changes of the ac field are quasi-adiabatic, the magnetization dynamics represent the so-called switching regime meaning that the magnetization may reverse due to the cooperative shuttling action of thermal agitation and applied field. Here, the DMH loop area decreases as the antiferromagnetic parameter ζ increases. Moreover, the coercivity, the remanent magnetization, and the saturation magnetization strongly depend on σ so that considerable variations in the area and shape of loops exist at low frequencies. At high frequencies, $\omega\tau_N \gg 1$, the DMH is mainly due to the absorption and dispersion in the "intrawell" and AFMR modes. Thus, the DMH arising from a high-frequency periodic signal may be evaluated permitting quantitative analysis of ultrafast switching of the magnetization in nanoscale antiferromagnets. At $\omega \sim \omega_{pr}$, the DMH occurs due to the *resonant* behavior of the nonlinear response, and under such conditions, the switching may be termed "resonant," leading naturally to the concept of *resonant switching of the magnetization*.[28–31] Since the resonant DMH occurs at very high (GHz) frequencies, the magnetization switching is, for the most part, governed by the frequency of the external driving field. Hence, the magnetization may be advantageously switched in this situation because the field needed to reverse it is then much smaller than the quasi-static coercive force. Here, the phase difference δ between $\mu_H(t)$ and $H(t)$, governing *loop orientation*, may undergo a pronounced variation. In particular, the phase difference δ may exceed $\pi/2$ as typical of a resonant process.[28–31] Obviously, this effect does not exist at low and intermediate frequencies, where relaxation processes dominate and δ is always less than $\pi/2$.

The shape and area of the DMH loops alter as the antiferromagnetic parameter ζ varies (see Figs. 5 and 6). In particular, as seen in Fig. 6, A_n strongly depends on temperature, namely, on increasing σ, i.e., decreasing temperature, the loop area initially increases, reaches a maximum, and then decreases. Furthermore, at low σ (high temperatures), the behavior of A_n for antiferromagnetic and ferromagnetic nanoparticles is very similar, while for large $\sigma > 10$, it can differ substantially. Figure 7 shows the behavior of the area A_n, Eq. (15), as a function of the ac field ξ for various anisotropy (inverse temperature) parameters $\sigma \sim T^{-1}$. For a *weak* ac field, the DMH loops are ellipses with area A_n given by Eq. (15); the behavior of $A_n \sim -\mathrm{Im}(m_1^1)$ being similar to that of

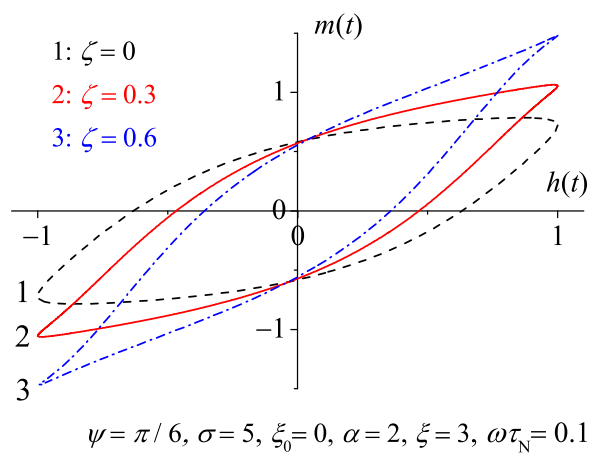

FIG. 5. DMH loops for various antiferromagnetic parameters ζ at $\omega\tau_N = 0.1$, $\sigma = 5$, $\alpha = 2$, $\psi = \pi/6$, $\xi = 3$, and $\xi_0 = 0$.

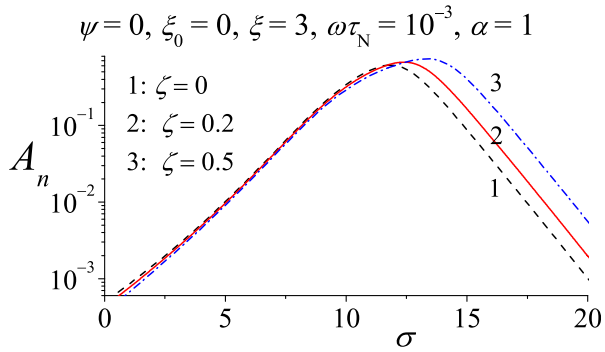

FIG. 6. Area A_n of the DMH loop vs. the anisotropy (inverse temperature) parameter $\sigma \sim T^{-1}$ for various antiferromagnetic parameters ζ at $\xi = 3$, $\alpha = 1$, and $\xi_0 = 0$.

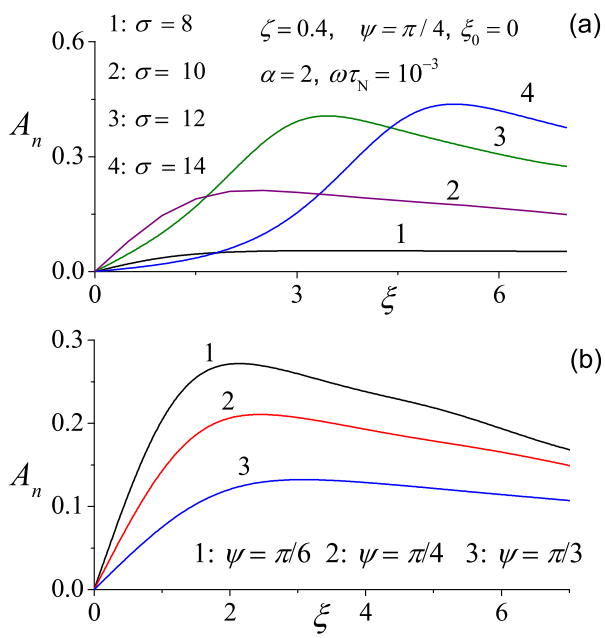

FIG. 7. Area A_n of the DMH loop vs. the ac field ξ: (a) for various barrier parameters $\sigma = 8, 10, 12, 14$ with the antiferromagnetic parameter $\zeta = 0.4$, dc field parameter $\xi_0 = 0$, frequency $\omega\tau_N = 10^{-3}$, and damping $\alpha = 2$; (b) angles $\psi = \pi/6, \pi/4, \pi/3$.

the magnetic loss $-\mathrm{Im}[\chi(\omega)]$ [cf. Eq. (14)]. In *strong* ac fields, $\xi > 1$, the DMH area alters substantially (see Fig. 7); nevertheless, A_n is still determined by $-\mathrm{Im}(m_1^1)$ [cf. Eq. (15)] with maxima appearing at strong fields, $\xi \geq 2$.

IV. CONCLUSION

The nonlinear forced ac stationary response of antiferromagnetic nanoparticles in superimposed ac and dc bias external magnetic fields is studied via continuous diffusion model.[5] It is shown that the nonlinear dynamic susceptibility and DMH in an ac field applied at an angle to the easy axis of the particle, so that the axial symmetry is broken, are very sensitive to both the ac field orientation and amplitude owing to the coupling induced by the symmetry breaking driving field between the precession of the magnetic moment and its thermally activated reversal. This explains why the nonlinear ac stationary response of antiferromagnetic nanoparticles is very sensitive to damping representing a signature of the coupling between the longitudinal and precessional modes of the magnetization just as nanoscale ferromagnets.[26–32] Furthermore, it is found that under appropriate conditions a small (in comparison with that of internal anisotropy) bias dc field can strongly affect the shape of the DMH loops in antiferromagnetic nanoparticles. This result implies that by varying the dc bias field strength, one may control the heat production (specific power loss) in a nanoparticle. Since the results are valid for ac fields of *arbitrary* strength and orientation, they provide a rigorous basis for the treatment of the nonlinear ac stationary response of antiferromagnetic nanoparticles in strong ac fields, where perturbation theory is no longer valid. Our calculations of the nonlinear response of an individual antiferromagnetic nanoparticle can be generalized to calculate the average magnetic moment of an assembly of randomly oriented noninteracting nanoparticles by averaging over particle easy axis orientations as described in detail in Ref. 27. We have also assumed that all the particles are identical and interparticle interactions are negligible. In order to account for the polydispersity, it is necessary to average over the appropriate distribution function over the particle volumes. The neglect of interparticle interactions in the present model suggests that the results apply only to systems, where interactions are ignored, such as individual nanoparticles and dilute solid suspensions of nanoparticles.

ACKNOWLEDGMENTS

We thank W. T. Coffey, W. Dowling, and P. M. Déjardin for a critical reading of the paper and useful comments and suggestions. We would like to thank FP7-PEOPLE-Marie Curie Actions-International Research Staff Exchange Scheme (Project No. 295196 DMH) for financial support. S. V. Titov also acknowledges the financial support of the program "Mechnikov" (the Embassy of France in Russia).

APPENDIX: MATRIX CONTINUED FRACTION SOLUTION OF EQ. (5) FOR THE AC STATIONARY RESPONSE

The time-dependent coefficients $w_{nm}(t)$, $x_{nm}(t)$, etc., in Eq. (5) can be presented as

$$w_{nm}(t) = w_{nm}^0 + w_{nm}^1(e^{i\omega t} + e^{-i\omega t}) + w_{nm}^2(e^{2i\omega t} + e^{-2i\omega t}),$$
$$x_{nm}(t) = x_{nm}^0 + x_{nm}^1(e^{i\omega t} + e^{-i\omega t}) + x_{nm}^2(e^{2i\omega t} + e^{-2i\omega t}),$$
$$y_{nm}(t) = y_{nm}^0 + y_{nm}^1(e^{i\omega t} + e^{-i\omega t}) + y_{nm}^2(e^{2i\omega t} + e^{-2i\omega t}),$$

etc., where the various time-independent coefficients w_{nm}^i, x_{nm}^i, etc., are given by

$$x_{nm}^0 = -\frac{n(n+1)}{2} - i\frac{\xi_0 m\gamma_3}{2\alpha} + \left[\frac{\zeta}{8}\left(2\xi_0^2 + \xi^2\right)\left(1 - 3\gamma_3^2\right) + \sigma\right]\frac{n(n+1) - 3m^2}{(2n-1)(2n+3)},$$

$$x_{nm}^{1} = -i\frac{\xi m\gamma_3}{4\alpha} + \frac{\zeta\xi_0\xi}{4}\left(1-3\gamma_3^2\right)\frac{n(n+1)-3m^2}{(2n-1)(2n+3)},$$

$$x_{nm}^{2} = \frac{\zeta\xi^2\left(1-3\gamma_3^2\right)\left[n(n+1)-3m^2\right]}{16(2n-1)(2n+3)},$$

$$x_{nm}^{-0} = (\gamma_1+i\gamma_2)\left[\frac{3(2m-1)\zeta\left(2\xi_0^2+\xi^2\right)\gamma_3}{8(2n-1)(2n+3)} - \frac{i\xi_0}{4\alpha}\right]\sqrt{(1+n-m)(n+m)},$$

$$x_{nm}^{-1} = (\gamma_1+i\gamma_2)\left[\frac{3(2m-1)\zeta\xi_0\xi\gamma_3}{4(2n-1)(2n+3)} - \frac{i\xi}{8\alpha}\right]\sqrt{(1+n-m)(n+m)},$$

$$x_{nm}^{-2} = (\gamma_1+i\gamma_2)\frac{3(2m-1)\zeta\xi^2\gamma_3}{16(2n-1)(2n+3)}\sqrt{(1+n-m)(n+m)},$$

$$x_{nm}^{--0} = \frac{3\zeta\left(2\xi_0^2+\xi^2\right)(\gamma_1+i\gamma_2)^2}{16(2n-1)(2n+3)}\sqrt{(1+n-m)(2+n-m)(-1+n+m)(n+m)},$$

$$x_{nm}^{--1} = \frac{3\zeta\xi\xi_0(\gamma_1+i\gamma_2)^2}{8(2n-1)(2n+3)}\sqrt{(1+n-m)(2+n-m)(-1+n+m)(n+m)},$$

$$x_{nm}^{--2} = \frac{3\zeta\xi^2(\gamma_1+i\gamma_2)^2}{32(2n-1)(2n+3)}\sqrt{(1+n-m)(2+n-m)(-1+n+m)(n+m)},$$

$$y_{nm}^{0} = -\left(\frac{\xi_0}{2}\gamma_3 n + \frac{im}{\alpha}\left[\sigma + \frac{\zeta\left(2\xi_0^2+\xi^2\right)\left(1-3\gamma_3^2\right)}{8}\right]\right)\sqrt{\frac{(n+1)^2-m^2}{(2n+1)(2n+3)}},$$

$$y_{nm}^{1} = -\frac{\xi}{4}\left[n\gamma_3 + \frac{im\zeta\xi_0\left(1-3\gamma_3^2\right)}{\alpha}\right]\sqrt{\frac{(n+1)^2-m^2}{(2n+1)(2n+3)}},$$

$$y_{nm}^{2} = -\frac{im\zeta\xi^2\left(1-3\gamma_3^2\right)}{16\alpha}\sqrt{\frac{(n+1)^2-m^2}{(2n+1)(2n+3)}},$$

$$y_{nm}^{-0} = (\gamma_1+i\gamma_2)\left[\frac{i(n+2m)\zeta\left(2\xi_0^2+\xi^2\right)\gamma_3}{8\alpha} - \frac{n\xi_0}{4}\right]\sqrt{\frac{(1+n-m)(2+n-m)}{(1+2n)(3+2n)}},$$

$$y_{nm}^{-1} = (\gamma_1+i\gamma_2)\left[\frac{2i\zeta\xi_0\xi\gamma_3}{4\alpha}(n+2m) - \frac{n\xi}{8}\right]\sqrt{\frac{(1+n-m)(2+n-m)}{(1+2n)(3+2n)}},$$

$$y_{nm}^{-2} = \frac{i\zeta\xi^2\gamma_3(\gamma_1+i\gamma_2)(n+2m)}{16\alpha}\sqrt{\frac{(1+n-m)(2+n-m)}{(1+2n)(3+2n)}},$$

$$y_{nm}^{--0} = \frac{i\zeta\left(2\xi_0^2+\xi^2\right)(\gamma_1+i\gamma_2)^2}{16\alpha}\sqrt{\frac{(1+n-m)(2+n-m)(3+n-m)(n+m)}{(1+2n)(3+2n)}},$$

$$y_{nm}^{--1} = \frac{i\zeta\xi_0\xi(\gamma_1+i\gamma_2)^2}{8\alpha}\sqrt{\frac{(1+n-m)(2+n-m)(3+n-m)(n+m)}{(1+2n)(3+2n)}},$$

$$y_{nm}^{--2} = \frac{i\zeta\xi^2(\gamma_1+i\gamma_2)^2}{32\alpha}\sqrt{\frac{(1+n-m)(2+n-m)(3+n-m)(n+m)}{(1+2n)(3+2n)}},$$

$$w_{nm}^{0} = \left(\frac{\gamma_3\xi_0}{2}(n+1) - \frac{im}{\alpha}\left[\frac{\zeta\left(2\xi_0^2+\xi^2\right)\left(1-3\gamma_3^2\right)}{8} + \sigma\right]\right)\sqrt{\frac{n^2-m^2}{4n^2-1}},$$

$$w_{nm}^{1}=\frac{\xi}{4}\left[\gamma_3(n+1)-\frac{im\xi_0\zeta}{\alpha}\left(1-3\gamma_3^2\right)\right]\sqrt{\frac{n^2-m^2}{4n^2-1}},$$

$$w_{nm}^{2}=-\frac{im\zeta\xi^2\left(1-3\gamma_3^2\right)}{16\alpha}\sqrt{\frac{n^2-m^2}{4n^2-1}},$$

$$w_{nm}^{-0}=-(\gamma_1+i\gamma_2)\left[\xi_0\frac{n+1}{4}-\frac{i(1-2m+n)\zeta\left(2\xi_0^2+\xi^2\right)\gamma_3}{8\alpha}\right]\sqrt{\frac{(n+m)(n+m-1)}{4n^2-1}},$$

$$w_{nm}^{-1}=-(\gamma_1+i\gamma_2)\left[\xi\frac{n+1}{8}-\frac{i(1-2m+n)\zeta\xi_0\xi\gamma_3}{4\alpha}\right]\sqrt{\frac{(n+m)(n+m-1)}{4n^2-1}},$$

$$w_{nm}^{-2}=\frac{i(1-2m+n)\zeta\xi^2\gamma_3(\gamma_1+i\gamma_2)}{16\alpha}\sqrt{\frac{(n+m)(n+m-1)}{4n^2-1}},$$

$$w_{nm}^{--0}=-\frac{i\zeta\left(2\xi_0^2+\xi^2\right)(\gamma_1+i\gamma_2)^2}{16\alpha}\sqrt{\frac{(n+m-2)(n+m-1)(1+n-m)(n+m)}{4n^2-1}},$$

$$w_{nm}^{--1}=-\frac{i\zeta\xi\xi_0(\gamma_1+i\gamma_2)^2}{8\alpha}\sqrt{\frac{(n+m-2)(n+m-1)(1+n-m)(n+m)}{4n^2-1}},$$

$$w_{nm}^{--2}=-\frac{i\zeta\xi^2(\gamma_1+i\gamma_2)^2}{32\alpha}\sqrt{\frac{(n+m-2)(n+m-1)(1+n-m)(n+m)}{4n^2-1}},$$

$$z_{nm}^{0}=-\left[\frac{\zeta\left(2\xi_0^2+\xi^2\right)}{8}\left(1-3\gamma_3^2\right)+\sigma\right]\frac{n}{2n+3}\sqrt{\frac{\left[(n+1)^2-m^2\right]\left[(n+2)^2-m^2\right]}{(2n+1)(2n+5)}},$$

$$z_{nm}^{1}=-\frac{n\zeta\xi_0\xi\left(1-3\gamma_3^2\right)}{4(2n+3)}\sqrt{\frac{\left[(n+1)^2-m^2\right]\left[(n+2)^2-m^2\right]}{(2n+1)(2n+5)}},$$

$$z_{nm}^{2}=\frac{n\zeta\xi^2\left(3\gamma_3^2-1\right)}{16(2n+3)}\sqrt{\frac{\left[(n+1)^2-m^2\right]\left[(n+2)^2-m^2\right]}{(2n+1)(2n+5)}},$$

$$z_{nm}^{-0}=\frac{n\left(2\xi_0^2+\xi^2\right)\zeta(\gamma_1+i\gamma_2)\gamma_3}{4(2n+3)}\sqrt{\frac{\left[(n+1)^2-m^2\right](n-m+2)(3+n-m)}{(2n+1)(2n+5)}},$$

$$z_{nm}^{-1}=\frac{n\xi\xi_0\zeta(\gamma_1+i\gamma_2)\gamma_3}{2(2n+3)}\sqrt{\frac{\left[(n+1)^2-m^2\right](n-m+2)(3+n-m)}{(2n+1)(2n+5)}},$$

$$z_{nm}^{-2}=\frac{n\zeta\xi^2(\gamma_1+i\gamma_2)\gamma_3}{8(2n+3)}\sqrt{\frac{\left[(n+1)^2-m^2\right](n-m+2)(3+n-m)}{(2n+1)(2n+5)}},$$

$$z_{nm}^{--0}=\frac{n\zeta\left(2\xi_0^2+\xi^2\right)(\gamma_1+i\gamma_2)^2}{16(2n+3)}\sqrt{\frac{(n+1-m)(2+n-m)(3+n-m)(4+n-m)}{(2n+1)(2n+5)}},$$

$$z_{nm}^{--1}=\frac{n\xi\xi_0\zeta(\gamma_1+i\gamma_2)^2}{8(2n+3)}\sqrt{\frac{(n+1-m)(2+n-m)(3+n-m)(4+n-m)}{(2n+1)(2n+5)}},$$

$$z_{nm}^{--2}=\frac{n\zeta\xi^2(\gamma_1+i\gamma_2)^2}{32(2n+3)}\sqrt{\frac{(n+1-m)(2+n-m)(3+n-m)(4+n-m)}{(2n+1)(2n+5)}},$$

$$v_{nm}^{0} = \left[\frac{\zeta\left(2\xi_0^2+\xi^2\right)}{8}\left(1-3\gamma_3^2\right)+\sigma\right]\frac{n+1}{2n-1}\sqrt{\frac{\left[(n-1)^2-m^2\right](n^2-m^2)}{(2n+1)(2n-3)}},$$

$$v_{nm}^{1} = \frac{(n+1)\zeta\xi_0\xi\left(1-3\gamma_3^2\right)}{4(2n-1)}\sqrt{\frac{\left[(n-1)^2-m^2\right](n^2-m^2)}{(2n+1)(2n-3)}},$$

$$v_{nm}^{2} = \frac{(n+1)\zeta\xi^2\left(1-3\gamma_3^2\right)}{16(2n-1)}\sqrt{\frac{\left[(n-1)^2-m^2\right](n^2-m^2)}{(2n+1)(2n-3)}},$$

$$v_{nm}^{-0} = \frac{(n+1)\zeta\left(2\xi_0^2+\xi^2\right)(\gamma_1+i\gamma_2)\gamma_3}{4(2n-1)}\sqrt{\frac{(n+m-2)(n+m-1)(n^2-m^2)}{(2n+1)(2n-3)}},$$

$$v_{nm}^{-1} = \frac{(n+1)\zeta\xi_0\xi(\gamma_1+i\gamma_2)\gamma_3}{2(2n-1)}\sqrt{\frac{(n+m-2)(n+m-1)(n^2-m^2)}{(2n+1)(2n-3)}},$$

$$v_{nm}^{-2} = \frac{(n+1)\zeta\xi^2(\gamma_1+i\gamma_2)\gamma_3}{8(2n-1)}\sqrt{\frac{(n+m-2)(n+m-1)(n^2-m^2)}{(2n+1)(2n-3)}},$$

$$v_{nm}^{--0} = -\frac{(n+1)\zeta\left(2\xi_0^2+\xi^2\right)(\gamma_1+i\gamma_2)^2}{16(2n-1)}\sqrt{\frac{(n+m-3)(n+m-2)(-1+n+m)(n+m)}{(2n+1)(2n-3)}},$$

$$v_{nm}^{--1} = -\frac{(n+1)\zeta\xi_0\xi(\gamma_1+i\gamma_2)^2}{4(2n-1)}\sqrt{\frac{(n+m-3)(n+m-2)(-1+n+m)(n+m)}{(2n+1)(2n-3)}},$$

$$v_{nm}^{--2} = -\frac{(n+1)\zeta\xi^2(\gamma_1+i\gamma_2)^2}{32(2n-1)}\sqrt{\frac{(n+m-3)(n+m-2)(-1+n+m)(n+m)}{(2n+1)(2n-3)}}.$$

The coefficients with the superscripts + and ++ can be calculated according to the rule: $a_{nm}^{+} = (a_{n-m}^{-})^*$ and $a_{nm}^{++} = (a_{n-m}^{--})^*$.

The stationary ac response can be calculated from the formally exact matrix continued fraction solution because Eq. (5) can be rearranged as matrix three-term recurrence relations

$$\mathbf{Q}_1\mathbf{C}_1(\omega)+\mathbf{Q}_1^{+}\mathbf{C}_2(\omega)=\mathbf{R}, \tag{A1}$$

$$\mathbf{Q}_n(\omega)\mathbf{C}_n(\omega)+\mathbf{Q}_n^{+}\mathbf{C}_{n+1}(\omega)+\mathbf{Q}_n^{-}\mathbf{C}_{n-1}(\omega)=0,\ n=2,3,..., \tag{A2}$$

$$\mathbf{C}_1 = \begin{pmatrix} \vdots \\ \mathbf{c}_n^{-2}(\omega) \\ \mathbf{c}_n^{-1}(\omega) \\ \mathbf{c}_n^{0}(\omega) \\ \mathbf{c}_n^{1}(\omega) \\ \mathbf{c}_n^{2}(\omega) \\ \vdots \end{pmatrix}, \quad \mathbf{c}_n^{k}(\omega) = \begin{pmatrix} c_{2n-2n}^{k}(\omega) \\ \vdots \\ c_{2n2n}^{k}(\omega) \\ c_{2n-1-2n+1}^{k}(\omega) \\ \vdots \\ c_{2n-12n-1}^{k}(\omega) \end{pmatrix},$$

with $\mathbf{c}_0(\omega) = (c_{00}^{0})$. Here, $c_{lm}^{k}(\omega)$ are the Fourier coefficients in the Fourier series in the time. The elements of the three-diagonal supermatrixes $\mathbf{Q}_n$ and $\mathbf{Q}_n^{\pm}$ are defined as

$$[\mathbf{Q}_n^{\pm}]_{lm} = \delta_{l-2m}\mathbf{r}_n^{\pm} + \delta_{l-1m}\mathbf{p}_n^{\pm} + \delta_{lm}\mathbf{q}_n^{\pm} + \delta_{l+1m}\mathbf{p}_n^{\pm} + \delta_{l+2m}\mathbf{r}_n^{\pm},$$

$$[\mathbf{Q}_n]_{lm} = \delta_{l-2m}\mathbf{r}_n + \delta_{l-1m}\mathbf{p}_n + \delta_{lm}(\mathbf{q}_n - im\tau_{\mathrm{N}}\omega\mathbf{I}) + \delta_{l+1m}\mathbf{p}_n + \delta_{l+2m}\mathbf{r}_n,$$

and

$$\mathbf{R} = -\mathbf{Q}_1^{-}\mathbf{C}_0 = -\frac{1}{\sqrt{4\pi}}\begin{pmatrix} \vdots \\ \mathbf{0} \\ \mathbf{r}_1^{-} \\ \mathbf{p}_1^{-} \\ \mathbf{q}_1^{-} \\ \mathbf{p}_1^{-} \\ \mathbf{r}_1^{-} \\ \mathbf{0} \\ \vdots \end{pmatrix},$$

where δ_{lm} is Kronecker's delta; the supermatrixes $\mathbf{q}_n^-, \mathbf{q}_n, \mathbf{q}_n^+, \mathbf{p}_n^-, \mathbf{p}_n, \mathbf{p}_n^+, \mathbf{r}_n^-, \mathbf{r}_n, \mathbf{r}_n^+$ are defined in Ref. 27, and the column vectors $\mathbf{c}_1^k(\omega)$, $\mathbf{p}_1^-$, $\mathbf{q}_1^-$, and $\mathbf{r}_1^-$ are given by

$$\mathbf{p}_1^- = \begin{pmatrix} -\sqrt{3/40}\zeta\xi_0\xi(\gamma_1 - i\gamma_2)^2 \\ -\sqrt{3/10}\zeta\xi_0\xi(\gamma_1 - i\gamma_2)\gamma_3 \\ \zeta\xi_0\xi(1 - 3\gamma_3^2)/\sqrt{20} \\ \sqrt{3/10}\zeta\xi_0\xi(\gamma_1 + i\gamma_2)\gamma_3 \\ -\sqrt{3/40}\zeta\xi_0\xi(\gamma_1 + i\gamma_2)^2 \\ \sqrt{1/24}\xi(\gamma_1 - i\gamma_2)\sigma \\ \xi\gamma_3/\sqrt{12} \\ -\sqrt{1/24}\xi(\gamma_1 + i\gamma_2) \end{pmatrix},$$

$$\mathbf{q}_1^- = \begin{pmatrix} -\sqrt{3/160}\zeta(2\xi_0^2 + \xi^2)(\gamma_1 - i\gamma_2)^2 \\ -\sqrt{3/40}\zeta(2\xi_0^2 + \xi^2)(\gamma_1 - i\gamma_2)\gamma_3 \\ [2\sigma + \zeta(2\xi_0^2 + \xi^2)(1 - 3\gamma_3^2)/4]/\sqrt{5} \\ \sqrt{3/40}\zeta(2\xi_0^2 + \xi^2)(\gamma_1 + i\gamma_2)\gamma_3 \\ -\sqrt{3/160}\zeta(2\xi_0^2 + \xi^2)(\gamma_1 + i\gamma_2)^2 \\ \sqrt{1/6}\xi_0(\gamma_1 - i\gamma_2) \\ \xi_0\gamma_3/\sqrt{3} \\ -\sqrt{1/6}\xi_0(\gamma_1 + i\gamma_2) \end{pmatrix},$$

$$\mathbf{r}_1^- = \frac{\xi^2\zeta}{16}\sqrt{\frac{6}{5}}\begin{pmatrix} -(\gamma_1 - i\gamma_2)^2 \\ -2(\gamma_1 - i\gamma_2)\gamma_3 \\ 2(1 - 3\gamma_3^2)/\sqrt{6} \\ 2(\gamma_1 + i\gamma_2)\gamma_3 \\ -(\gamma_1 + i\gamma_2)^2 \\ 0 \\ 0 \\ 0 \end{pmatrix}.$$

The exact solution of Eqs. (A1) and (A2) is then rendered by the matrix continued fraction

$$\mathbf{C}_1 = -\mathbf{S}_1\,\mathbf{Q}_1^{-}\mathbf{C}_0, \tag{A3}$$

where the infinite matrix continued fraction $\mathbf{S}_1$ is defined by the recurrence equation

$$\mathbf{S}_n = -[\mathbf{Q}_n + \mathbf{Q}_n^{+}\mathbf{S}_{n+1}\mathbf{Q}_{n+1}^{-}]^{-1}.$$

Having calculated the Fourier amplitudes $c_{lm}^k(\omega)$ from Eq. (A3), we can evaluate the Fourier amplitudes $m_1^k(\omega)$ in Eq. (9) for the average dipole moment $\mu_H(t)$, Eq. (8), as

$$\begin{aligned} m_1^k(\omega) = {} & \frac{2\zeta\xi_0}{3}\delta_{0k} + \frac{\zeta\xi}{6}(\delta_{1k} + \delta_{-1k}) + \sqrt{\frac{2\pi}{3}}\Big\{\sqrt{2}\cos\psi c_{10}^k(\omega) + \sin\psi\big[c_{1-1}^k(\omega) - c_{11}^k(\omega)\big]\Big\} \\ & - \zeta\sqrt{\frac{2\pi}{15}}\Bigg\{\sqrt{\frac{2}{3}}\big(3\cos^2\psi - 1\big)\Big(\xi_0 c_{20}^k(\omega) + \frac{\xi}{2}\big[c_{20}^{k-1}(\omega) + c_{20}^{k+1}(\omega)\big]\Big) \\ & + \sin 2\psi\Big(\xi_0\big[c_{2-1}^k(\omega) - c_{21}^k(\omega)\big] + \frac{\xi}{2}\big[c_{2-1}^{k-1}(\omega) + c_{2-1}^{k+1}(\omega) - c_{21}^{k-1}(\omega) - c_{21}^{k+1}(\omega)\big]\Big) \\ & + \sin^2\psi\Big(\xi_0\big[c_{22}^k(\omega) + c_{2-2}^k(\omega)\big] + \frac{\xi}{2}\big[c_{22}^{k-1}(\omega) + c_{22}^{k+1}(\omega) + c_{2-2}^{k-1}(\omega) + c_{2-2}^{k+1}(\omega)\big]\Big)\Bigg\}. \end{aligned} \tag{A4}$$

Here, we have assumed without loss of generality that the direction cosines of the vector $\mathbf{H}_0$ are $\gamma_1 = \sin\psi$, $\gamma_2 = 0$, $\gamma_3 = \cos\psi$ and have used the known definitions of the spherical harmonics of the first and second rank and equations for $\langle\cos\Theta\rangle(t)$ and $\langle\cos^2\Theta\rangle(t)$ expressed via the statistical moments $\langle Y_{1m}\rangle(t)$ and $\langle Y_{2m}\rangle(t)$ as

$$\langle \cos\Theta\rangle(t) = \sqrt{\frac{2\pi}{3}}\Big(\sqrt{2}\cos\psi\langle Y_{10}\rangle(t) + \sin\psi\big[\langle Y_{1-1}\rangle(t) - \langle Y_{11}\rangle(t)\big]\Big), \tag{A5}$$

$$\langle \cos^2\Theta\rangle(t) = \frac{1}{3} + \sqrt{\frac{2\pi}{15}}\Big\{\sqrt{2/3}\big(3\cos^2\psi - 1\big)\langle Y_{20}\rangle(t) + \sin 2\psi\big[\langle Y_{2-1}\rangle(t) - \langle Y_{21}\rangle(t)\big] + \sin^2\psi\big[\langle Y_{22}\rangle(t) + \langle Y_{2-2}\rangle(t)\big]\Big\}. \tag{A6}$$

[1]C. D. Mee, *The Physics of Magnetic Recording* (North Holland, Amsterdam, 1986).
[2]*Handbook of Advanced Magnetic Materials*, edited by Y. Liu, D. J. Sellmyer, and D. Shindo (Springer, New York, 2006), Vols. I and II.
[3]*Magnetic Nanoparticles*, edited by S. P. Gubin (Wiley, New York, 2009).
[4]A. Pankhurst, N. K. T. Thanh, S. K. Jones, and J. Dobson, J. Phys. D: Appl. Phys. **42**, 224001 (2009).
[5]J. Carrey, B. Mehdaoui, and M. Respaud, J. Appl. Phys. **109**, 083921 (2011); N. A. Usov and B. Y. Liubimov, *ibid.* **112**, 023901 (2012).
[6]E. A. Rérigo, G. Hemery, O. Sandre, and F. J. Teran, Appl. Phys. Rev. **2**, 041302 (2015).
[7]L. Néel, Ann. Géophys. **5**, 99 (1949); C. R. Acad. Sci. Paris **228**, 664 (1949).
[8]C. P. Bean and J. D. Livingston, J. Appl. Phys. Suppl. **30**, 120S (1959).
[9]Yu. L. Raikher and V. I. Stepanov, J. Exp. Theor. Phys. **107**, 435 (2008) [Zh. Eksp. Teor. Fiz. **134**, 514 (2008)]; J. Phys.: Condens. Matter **20**, 204120 (2008).
[10]L. Néel, C. R. Acad. Sci. Paris **252**, 4075 (1961); **253**, 9 (1961); **253**, 203 (1961); **253**, 1286 (1961).
[11]W. F. Brown, Jr., Phys. Rev. **130**, 1677 (1963).
[12]W. F. Brown, Jr., IEEE Trans. Magn. **15**, 1196 (1979).
[13]L. D. Landau and E. M. Lifshitz, Phys. Z. Sowjetunion **8**, 153 (1935).
[14]T. L. Gilbert, Phys. Rev. **100**, 1243 (1955) (Abstract only; full report in: Armour Research Foundation Project No. A059, Supplementary Report, 1956). Reprinted in T. L. Gilbert, IEEE Trans. Magn. 40, 3443 (2004).
[15]M. S. Seehra and A. Punnoose, Phys. Rev. B **64**, 132410 (2001).
[16]C. Gilles, P. Bonville, H. Rakoto, J. M. Broto, K. K. W. Wong, and S. Mann, J. Magn. Magn. Mater. **241**, 430 (2002).
[17]L. Zhang, D. Xue, and C. Gao, J. Magn. Magn. Mater. **267**, 111 (2003).
[18]N. J. O. Silva, A. Millán, F. Palacio, E. Kampert, U. Zeitler, H. Rakoto, and V. S. Amaral, Phys. Rev. B **79**, 104405 (2009).
[19]Yu. L. Raĭkher, V. I. Stepanov, S. V. Stolyar, V. P. Ladygina, D. A. Balaev, L. A. Ishchenko, and M. Balasoiu, Fiz. Tverd. Tela **52**, 277 (2010) [Phys. Solid State **52**, 298 (2010)].
[20]D. A. Balaev, A. A. Krasikov, A. A. Dubrovskii, S. V. Semenov, O. A. Bayukov, S. V. Stolyar, R. S. Iskhakov, V. P. Ladygina, and L. A. Ishchenko, Zh. Eksp. Teor. Fiz. **146**, 546 (2014), [J. Exp. Theor. Phys. **119**, 479 (2014)].
[21]D. A. Varshalovitch, A. N. Moskalev, and V. K. Khersonskii, *Quantum Theory of Angular Momentum* (World Scientific, Singapore, 1988).
[22]W. T. Coffey and Yu. P. Kalmykov, *The Langevin Equation*, 3rd ed. (World Scientific, Singapore, 2012).
[23]B. Ouari and Yu. P. Kalmykov, Phys. Rev. B **83**, 064406 (2011).
[24]B. Ouari, S. Aktaou, and Yu. P. Kalmykov, Phys. Rev. B **81**, 024412 (2010).
[25]W. T. Coffey and Y. P. Kalmykov, J. Appl. Phys. **112**, 121301 (2012).
[26]J. L. García-Palacios and P. Svedlindh, Phys. Rev. Lett. **85**, 3724 (2000).
[27]S. V. Titov, P. M. Déjardin, H. El Mrabti, and Yu. P. Kalmykov, Phys. Rev. B **82**, 100413(R) (2010).
[28]I. S. Poperechny, Yu. L. Raikher, and V. I. Stepanov, Phys. Rev. B **82**, 174423 (2010).
[29]P. M. Déjardin, Yu. P. Kalmykov, B. E. Kashevsky, H. El Mrabti, I. S. Poperechny, Yu. L. Raikher, and S. V. Titov, J. Appl. Phys. **107**, 073914 (2010).
[30]H. El Mrabti, S. V. Titov, P. M. Déjardin, and Yu. P. Kalmykov, J. Appl. Phys. **110**, 023901 (2011).
[31]H. El Mrabti, P. M. Déjardin, S. V. Titov, and Yu. P. Kalmykov, Phys. Rev. B **85**, 094425 (2012).
[32]G. T. Landi, J. Magn. Magn. Mater. **324**, 466 (2012); J. Appl. Phys. **111**, 043901 (2012).
[33]Yu. L. Raikher, V. I. Stepanov, and R. Perzynski, Physica B **343**, 262 (2004).
[34]Yu. L. Raikher and V. I. Stepanov, J. Magn. Magn. Mater. **300**, e311 (2006).
[35]Yu. L. Raikher and V. I. Stepanov, J. Magn. Magn. Mater. **320**, 2692 (2008).
[36]V. A. Ignatchenko and R. S. Gekht, Zh. Exp. Teor. Fiz. **67**, 1506 (1974) [Sov. Phys. JETP **40**, 750 (1975)].
[37]L. D. Landau and E. M. Lifshitz, *Mechanics*, 3rd ed. (Pergamon Press, London, 2000).